BIOCHEMISTRY
including biophysical chemistry & molecular biology

Article

pubs.acs.org/biochemistry

Binding of Islet Amyloid Polypeptide to Supported Lipid Bilayers and Amyloid Aggregation at the Membranes

Kenji Sasahara,*[,†] Kenichi Morigaki,[‡,§] Takashi Okazaki,[‡] and Daizo Hamada[†]

[†]Division of Structural Biology (G-COE), Department of Biochemistry and Molecular Biology, Graduate School of Medicine, Kobe University, Kobe 650-0017, Japan

[‡]National Institute of Advanced Industrial Science and Technology (AIST), Ikeda 563-8577, Japan

[§]Research Center for Environmental Genomics, Kobe University, Kobe 657-8501, Japan

Supporting Information

ABSTRACT: Amyloid deposition of human islet amyloid polypeptide (hIAPP) in the islets of Langerhans is closely associated with the pathogenesis of type II diabetes mellitus. Despite substantial evidence linking amyloidogenic hIAPP to loss of β-cell mass and decreased pancreatic function, the molecular mechanism of hIAPP cytotoxicity is poorly understood. We here investigated the binding of hIAPP and nonamyloidogenic rat IAPP to substrate-supported planar bilayers and examined the membrane-mediated amyloid aggregation. The membrane binding of IAPP in soluble and fibrillar states was characterized using quartz crystal microbalance with dissipation monitoring, revealing significant differences in the binding abilities among different species and conformational states of IAPP. Patterned model membranes composed of polymerized and fluid lipid bilayer domains were used to microscopically observe the amyloid aggregation of hIAPP in its membrane-bound state. The results have important implications for lipid-mediated aggregation following the penetration of hIAPP into fluid membranes. Using the fluorescence recovery after photobleaching method, we show that the processes of membrane binding and subsequent amyloid aggregation are accompanied by substantial changes in membrane fluidity and morphology. Additionally, we show that the fibrillar hIAPP has a potential ability to perturb the membrane structure in experiments of the fibril-mediated aggregation of lipid vesicles. The results obtained in this study using model membranes reveal that membrane-bound hIAPP species display a pronounced membrane perturbation ability and suggest the potential involvement of the oligomeic forms of hAPP in membrane dysfunction.

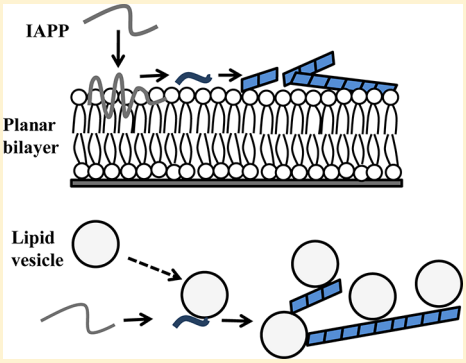

Human islet amyloid polypeptide (hIAPP) is a 37-residue peptide hormone, the major constituent of amyloid fibrils deposited in the pancreatic islets associated with type II diabetes mellitus (T2DM).[1−3] Insoluble fibrillar deposition of hIAPP in the extracellular space of pancreatic β-cells is observed in more than 90% of T2DM patients and strongly associated with β-cell degeneration and loss.[4,5] hIAPP is synthesized in pancreatic β-cells and cosecreted with insulin.[6] Although the exact physiological function of hIAPP remains under investigation, it is believed to control plasma glucose levels via regulation of glucagon and insulin secretion and gastric emptying.[7,8]

In vitro studies have shown that both hydrophobic and electrostatic interactions play an important role in amyloid fibril formation.[9] It is well established that highly amyloidogenic hIAPP is spontaneously converted to fibrillar structures through amyloid nucleation when diluted into physiological buffers containing salts.[10] The conversion is accelerated by the presence of lipid membranes, particularly those containing negative charges. Although the molecular mechanism of such an acceleration remains elusive, it is possible that lipid membrane-induced changes in the conformation of polypeptides might help the nucleation of amyloid fibrils.[11−14]

Several studies have shown that early amyloid oligomers or prefibrillar species of hIAPP are more toxic to cultured cells than its mature amyloid fibrils.[15−20] In contrast, mouse and rat IAPP are much less toxic than hIAPP.[12,21−23] This lower toxicity is usually attributed to the inability of IAPPs to convert to amyloid fibrils because of the presence of three prolines at positions 25, 28, and 29 (Figure 1a). Furthermore, mice and rats do not naturally develop T2DM, but transgenic rats (or mice) that express hIAPP have a strong propensity to develop T2DM characterized by amyloidogenesis and loss of β-cell mass.[24] Currently, a prevailing view is that aggregated hIAPP has cytotoxic properties and that the interactions of amyloidogenic hIAPP with β-cell membranes play a significant role in T2DM pathogenesis.[25,26]

Generally, membrane damage induced by the formation of pore-like channels in the lipid membranes or detergent-like action of soluble amyloid oligomers or their prefibrillar species is thought to provoke cellular dysfunction or death in T2DM, Alzheimer's disease, Parkinson's disease, and other amyloid

Received: April 27, 2012
Revised: August 9, 2012
Published: August 9, 2012

(a)

Human KCNTATCATQRLANFLVHSSNNFGAI LSSTNVGSNTY

Rat KCNTATCATQRLANFLVRSSNNLGPVLPPTNVGSNTY

(b)

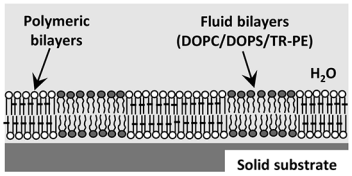

Figure 1. Comparison of sequences human and rat IAPP and schematic of the patterned lipid membrane. (a) The peptides are amidated at the C-terminus and have a disulfide bond between residues 2 and 7. The six amino acid residues colored red represent the differences between the two sequences. (b) The fabrication process of the patterned bilayers used in this study comprises four steps: (i) formation of a monomeric bilayer of the diacetylene phospholipid (DiynePC) on a solid substrate, (ii) lithographic photopolymerization by UV light, (iii) removal of the unpolymerized bilayers, and (iv) refilling the empty areas with new lipid bilayers. The chemical structure of DiynePC and its photopolymerization scheme can be found in the literature.[41−44]

diseases.[27−29] Besides, there is substantial evidence that signal cascades leading to apoptosis are triggered by amyloidogenic proteins causing cellular insults.[30−32] Despite recent efforts toward biophysical characterization of the different stages of amyloid aggregation,[13,33−36] we still lack the detailed characterization of membrane-mediated amyloid aggregation and the concomitant effects on various physicochemical properties of lipid membranes. In this context, it is an active area of research to elucidate the causes of membrane damage triggered by amyloidogenic IAPP and their role in the pathology of T2DM.[25,26]

Substrate-supported planar bilayers (SPBs) have been widely used as cell-surface models for investigating membrane characteristics in many studies ranging from the research on the properties and function of lipid bilayers to the examination of membrane−protein interactions.[37−40] Recently, Morigaki et al. have developed a novel micropatterning method for SPBs using a lithographic photopolymerization technique in which the polymerized bilayer of 1,2-bis(10,12-tricosadiynoyl)-*sn*-glycero-3-phosphocholine (DiynePC) forms an integrated matrix with embedded fluid bilayers (Figure 1b).[41−44] The polymeric lipid bilayer domains act not only as a barrier to confine fluid lipid bilayers in defined areas but also as a framework to support embedded membranes. The fluid bilayer domains retain the physicochemical properties such as lateral mobility of lipid molecules similar to those of cellular membranes. This patterned bilyer system was used in this study to examine the binding of hIAPP and rat IAPP (rIAPP) to fluid bilayer domains and to investigate the membrane-mediated amyloid aggregation. Moreover, quartz crystal microbalance with dissipation monitoring (QCM-D) and fluorescence recovery after photobleaching (FRAP) measurements were conducted to characterize the mass and viscoelastic properties of membrane-bound IAPP and the concomitant changes in membrane fluidity and integrity. Using lipid vesicles, we also investigated the affinity of fibrillar hIAPP for the membrane. We focused on how amyloid aggregation of hIAPP is induced at SPBs and its effect on membrane properties.

MATERIALS AND METHODS

Materials. Diacetylene phospholipid [1,2-bis(10,12-tricosadiynoyl)-*sn*-glycero-3-phosphocholine (DiynePC)], 1,2-dioleoyl-*sn*-glycero-3-phosphocholine (DOPC), 1,2-dimyristoyl-*sn*-glycero-3-phosphocholine (DMPC), and 1,2-dioleoyl-*sn*-glycero-3-phospho-L-serine (DOPS) were purchased from Avanti Polar Lipids, Inc. (Alabaster, AL). Texas Red 1,2-dihexadecanoyl-*sn*-glycero-phosphoethanolamine (TR-PE) and thioflavin T (ThT) were purchased from Molecular Probes (Eugene, OR) and Wako Pure Chemical Industries Ltd. (Osaka Japan), respectively. C-Terminally amidated synthetic IAPP of human and rat were purchased from Peptide Institute, Inc. (Osaka, Japan); their purity was >95% according to the elution pattern of reversed-phase high-performance liquid chromatography. All other chemicals were of reagent grade. The standard buffer [50 mM phosphate buffer (pH 7.2) and 100 mM sodium chloride] was passed through a filter (pore size, 0.22 μm) and used throughout the experiments. Pure (deionized and distilled) water was used for the preparation of all solutions.

Preparation of IAPP in the Soluble and Fibrillar States. IAPP was dissolved in dimethyl sulfoxide (DMSO) at 4 mg/mL and diluted with pure water to a concentration of 0.4 mg/mL (102 μM). Freshly diluted IAPP was used as the soluble form. Amyloid fibrils of hIAPP at 0.1 mg/mL (25.6 μM) were spontaneously formed in the standard buffer incubated at 37 °C overnight. IAPP solutions were used immediately after preparation. The solution conditions of IAPP are summarized in Table 1.

Table 1. Solution Conditions Used and States of IAPP

	solvent			
state of IAPP	buffer[a]	DMSO (%) (v/v)	pH	IAPP concentration (μM)
fibrillar hIAPP	+	0.68 (0.49)[c]	7.2	7.0 (5.0)[c]
soluble hIAPP	− (water)[b]	0.68 (0.49)	6.8−7.3	7.0 (5.0)
soluble rIAPP	− (water)[b]	0.68 (0.49)	6.8−7.3	7.0 (5.0)

[a]Consisting of 50 mM sodium phosphate and 100 mM NaCl (pH 7.2). [b]Pure water. [c]IAPP solutions at 5.0 and 7.0 μM contain DMSO at 0.49 and 0.68% (v/v), respectively.

Preparation of Lipid Vesicles and Formation of SPB. Stock solutions of DOPC, DOPS, and DMPC were prepared by dissolving the lipids in chloroform at a concentration of 10 mg/mL. In the experiments using SPBs, the DOPC/DOPS solution (4/1, w/w) was mixed with a TR-PE fluorescence marker in the same solvent at a molar concentration of 1.0% of the total amount of lipids. The lipid ratio was chosen because it resembles the composition of zwitterionic lipids and negatively charged lipids of the membrane of pancreatic islet cells.[45] After evaporation of chloroform under a stream of nitrogen gas, the dried film was kept for 4 h in a vacuum desiccator to remove any residual solvent. The film was hydrated in the standard buffer to yield a total lipid concentration of 1.0 mg/mL. After five freeze−thaw cycles, the resultant lipid suspension was stored in the dark at 4 °C. The lipid suspension was extruded 21 times through a polycarbonate filter (pore size, 50 nm) using a mini-extruder (Avanti Polar Lipids, Inc.) just before use. Vesicle suspensions in buffer were introduced into the glass

dx.doi.org/10.1021/bi300542g | *Biochemistry* 2012, 51, 6908−6919

substrate to form SPBs by a self-assembly process (vesicle fusion).

For turbidity measurements, dried films of four types of lipids [i.e., DOPC, DOPS, DOPC/DOPS (4/1), and DMPC] were similarly prepared without adding TR-PE and mixed with pure water to yield a lipid concentration of 10 mg/mL, followed by mild agitation to ensure complete mixing and hydration of lipids. The lipid suspensions were extruded 21 times through a filter (pore size, 100 nm).

QCM-D Measurements. QCM-D measurements were conducted using a Q-Sence D300 system with a QAFC 302 axial flow chamber (Q-sence, Göteborg, Sweden). Quartz crystals coated with a thin SiO_2 layer were used as the sensors (Q-sence). The sensor mounted to the measurement chamber was filled and equilibrated with degassed buffer. All injections (approximately 2 mL) of solutions were made by opening a valve between the container and the chamber, which allowed a gravitationally driven rapid exchange of the solutions covering the sensor. Prior to each measurement, the sensor crystals were cleaned by immersion in a 0.1 M sodium dodecyl sulfate (SDS) solution for 30 min at 30 °C, rinsed with pure water, dried with nitrogen, and subjected to UV/ozone treatment for 20 min (PL16-110, Sen Lights Corp., Toyonaka, Japan). During the measurements, the sensor crystal was oscillated at its resonance frequency of 5 MHz and three overtones (15, 25, and 35 MHz). Shifts in frequency (Δf), which measure the accumulation of mass onto the sensor surface, and dissipation (ΔD), which measures properties related to the viscoelastic properties of the adlayer, were monitored as a function of time. The interval for data acquisition was 0.4 s. The temperature during the experiments was kept at 21.8 °C. All data presented here were recorded at 25 MHz (i.e., the fifth overtone).

Substrate Cleaning. The substrates [microscopy glass slides (Matsunami, Osaka, Japan)] were cleaned using a commercial detergent solution [0.5% Hellmanex/water (Hellma, Mühlheim, Germany)], rinsed with pure water, immersed in an aqueous solution containing NH_4OH [0.23% (w/v)] and H_2O_2 [4.96% (w/v)] at 65 °C for 10 min, and rinsed again with pure water. The substrates were then dried in a vacuum oven for 30 min at 80 °C and further cleaned by UV/ozone treatment for 20 min.

Preparation of Patterned DiynePC Bilayers. DiynePC dissolved in pure water at 3.0 mM was subjected to five freeze–thaw cycles. The resulting lipid solution was homogenized by sonication for 1 min and deposited onto a glass slide to form a bilayer of DiynePC by a self-assembly process (vesicle fusion). Polymerization of DiynePC bilayers was conducted by UV irradiation using a mercury lamp (UVE-502SD, Ushio, Tokyo, Japan) as the light source. The intensity of applied UV was typically 10 mW/cm^2 at 254 nm, and the irradiation dose was 4 J/cm^2. The desired pattern was transferred to the DiynePC bilayer during polymerization by illuminating the sample through a mask (a quartz slide with a patterned chromium layer coating), which was placed directly on the bilayer.[43] After UV irradiation, nonpolymerized DiynePC molecules were removed from the substrate by immersion in a 0.1 M SDS solution at 30 °C for 30 min and rinsing with pure water. The patterned and polymerized DiynePC substrates were stored in pure water at 4 °C in the dark.

Incorporation of a DOPC/DOPS/TR-PE Suspension into the Corrals Surrounded by Polymerized DiynePC Bilayers. A vesicle suspension (DOPC/DOPS/TR-PE, total lipid concentration of 1 mg/mL, 150 μL) was brought into contact with the patterned DiynePC bilayer and incubated for 30 min at room temperature. The sample was rinsed extensively with pure water. Then, a flow cell was assembled; a coverslip was attached to the glass slide with the patterned bilayers using double-sided adhesive tapes, and a narrow space with an inlet and outlet was created over the patterned bilayers. To exchange the solutions covering the bilayer, solutions (150 μL) of the buffer or peptide (7 μM) were introduced using a micropipet at the inlet and sucked using a piece of filter paper at the outlet.

Fluorescence Microscopy Observation. Microscopic observations were made using an Olympus BX51WI upright microscope with a 60× water immersion objective (NA 0.90, Olympus) and a xenon lamp (AH2-RX-T, Olympus). Polymeric DiynePC bilayers were examined using an Olympus U-MNIBA2 filter set (excitation wavelength, 470–490 nm; emission wavelength, 510–550 nm). TR-PE fluorescence was examined using an Olympus U-MWIY2 filter set (excitation wavelength, 545–580 nm; emission wavelength, >610 nm). Thioflavin T fluorescence was examined using an Olympus U-MNBV2 filter set (excitation wavelength, 420–440 nm; emission wavelength, >475 nm). Fluorescence microscopy images were collected using a CCD camera (DP30BW, Olympus) and processed using MetaMorph (Molecular Devices, Sunnyvale, CA).

FRAP Analysis Using the Boundary Profile Evolution (BPE) Method. For the FRAP measurements, homogeneous SPBs without any pattern were used. A 150 μL aliquot of vesicle solution was pipetted onto a glass slide and incubated at room temperature for 30 min to form a lipid bilayer. After the bilayer was carefully rinsed with pure water, a flow cell was assembled, and solutions of the peptide and buffer were introduced into the cell in the same manner as in the experiments using the patterned bilayers. Fluorescence images of TR-PE in the lipid bilayer were acquired using a fluorescence microscope. Photobleaching was performed through a rectangular slit, keeping the shutter open for 30 s without an ND filter (at the full power of the lamp). Fluorescence recovery at the boundary region between the bleached and unbleached areas was monitored by taking 10 successive images after photobleaching (every 5 s for lipid membranes and every 15 s for lipid/IAPP membranes). The collective boundary profiles were fitted to a Gaussian error function (erf) using Origin (Origin Lab Corp., Northampton, MA) for determining diffusion depth w, which is defined as follows:

$$2\frac{F(x,t)-F_{\mathrm{bleached}}}{F_{\mathrm{unbleached}}-F_{\mathrm{bleached}}}=\mathrm{erf}\left(\frac{x-x_{\mathrm{b}}}{2w}\right)+1$$

$$w=\sqrt{Dt}$$

where $F(x, t)$ is the profile evolution with time t after photobleaching, F_{bleached} and $F_{\mathrm{unbleached}}$ are the fluorescence intensities of the bleached and unbleached regions, respectively, x_{b} is the position of the boundary, and $x - x_{\mathrm{b}}$ represents the distance to the boundary. w^2 values were plotted versus time t. The diffusion coefficient of fluorescent molecules D was determined from the slope of linear dependence.[44,46]

Turbidity Measurements. Turbidity measurements were conducted to investigate the kinetics of the binding reaction between hIAPP amyloid fibrils and lipid vesicles at pH 7.2 and 25 °C. The vesicles without TR-PE in pure water were diluted to the desired concentrations with the stock solutions of phosphate and NaCl at pH 7.2 (final buffer concentrations of 50 mM phosphate and 100 mM NaCl) before mixing with

amyloid fibrils. The fibril solution containing the same buffer was manually mixed with the vesicle solution in a test tube and agitated for 3 s using a benchtop vortex mixer. The mixed sample was transferred to a quartz cuvette (path length of 10 mm). Using a JASCO V-550 spectrophotometer (JASCO Co., Tokyo, Japan), time-dependent changes in solution turbidity were measured for 1 h as the apparent absorption at 600 nm (Abs_{600}). The time interval from the initiation of mixing to the first measurement was 40 s. The turbidity of the samples 24 h after mixing was measured following agitation for 3 s using the vortex mixer. The temperature of the sample was maintained at 25 ± 0.1 °C using a thermostatic water bath.

RESULTS

QCM-D Experiments. The formation of SPB and the subsequent exposure of the model membrane to IAPP solutions were monitored by QCM-D. A typical QCM-D profile obtained for vesicle fusion is shown in Figure 2a. At 240 s, the sensor surface was exposed to the vesicle solution (0.1 mg/mL), resulting in a rapid and large decrease in frequency, *f*, and an increase in energy dissipation, *D*. As the adsorbed vesicles spread and transformed into SPB, an increase in *f* was observed (between approximately 330 and 470 s) because the trapped water inside the vesicles was lost.[47,48] Simultaneously, the adsorbed layer became more rigid, and the dissipation approached zero. After the signals stabilized (>470 s), the sensor surface was rinsed with buffer to remove free vesicles and check for bilayer stability (mark 0 in Figure 2a), causing inappreciable changes in *f* and *D* corresponding to desorption of the free vesicles. The values for Δf (approximately 28 Hz) and ΔD (near zero) after the rinse corroborated the formation of the planar bilayer (Figure 2a), which are in agreement with previously published results.[44,47,49]

The QCM-D signals, resulting from exposure of SPB to the fibrillar hIAPP, soluble hIAPP, and soluble rIAPP, are shown in panels a–c of Figure 2, respectively. The buffer covering SPBs was replaced with each solvent of IAPP samples (see Table 1) (mark 1). This solution exchange caused the small shifts in *f* and *D* because of changes in the viscoelastic property of the aqueous phase covering the sensor. Then, the SPBs were exposed to IAPP solutions at 7 μM (mark 2). No detectable changes in *f* and *D* were observed in the case of hIAPP fibrils (Figure 2a). However, we observed a rapid decrease in *f* and a rapid increase in *D* when the soluble hIAPP solution was injected onto SPB (Figure 2b). With time (approximately 7400 s), the signals showed asymptotic curves typical of a saturable process. The injection of soluble rIAPP caused a quick, small decrease in *f* and a slight increase in *D* (Figure 2c). The signals stabilized much faster than those observed for soluble hIAPP.

The sensor surface was then rinsed with the solvent (mark 3), and the solvent was replaced with the buffer (mark 4). As shown in Figure 2a, the signals returned to the values obtained for the bilayer equilibrated with the buffer, which indicates that hIAPP fibrils have a low binding affinity for the membrane. On the other hand, we observed a rapid decrease in *f* and an increase in *D* in the experiment using soluble hIAPP, promptly followed by asymptotic behavior (Figure 2b). Of note, the shifts in *f* and *D* detected after buffer injection (mark 4) were larger than those corresponding to the buffer–solvent exchange (mark 1). This result indicates that a reaction associated with an increase in mass occurs upon addition of the buffer. Further injections of the buffer caused no pronounced signal changes (mark 5). Interestingly, in the experiment using rIAPP (Figure 2c), replacement of the solvent with the buffer caused an increase in both *f* and *D* (mark 4). Of note, the resulting value for Δf (approximately 25 Hz) after solution exchange (mark 4) is smaller than that (approximately 28 Hz) detected for bilayer formation under identical buffer conditions. Further addition of the buffer did not cause a noticeable Δf or ΔD (mark 5). As these results suggest that the addition of the buffer to the membrane-bound rIAPP might cause the loss of lipid from the bilayer, we proceeded to examine this process in our next experiment described below.

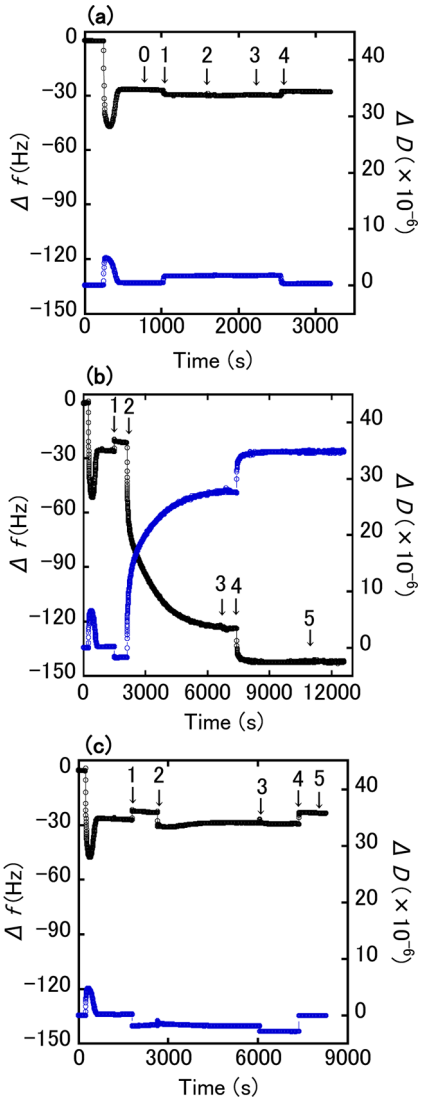

Figure 2. Binding of 7 μM IAPP to SPB analyzed by QCM-D. Changes in the resonant frequency (Δf, black traces) and dissipation (ΔD, blue traces) for the binding of three IAPP samples to SPB were monitored as a function of time: (a) amyloid fibrils of hIAPP, (b) soluble hIAPP, and (c) soluble rIAPP. Marks 0–5 represent times of injection (see the text).

In short, the comparative QCM-D profiles (Figure 2a–c) indicate that in contrast with the low binding affinity of hIAPP fibrils, the membrane binding affinity of soluble hIAPP is significant, with adsorption higher than that of nonamyloidogenic rIAPP. We repeated the same experiments with IAPP samples at 5 μM (different concentration). Binding characteristics very similar to those obtained at 7 μM were observed (Figure S1 of the Supporting Information).

dx.doi.org/10.1021/bi300542g | *Biochemistry* 2012, 51, 6908–6919

Binding of IAPP to Patterned Composite Membranes. Fluid lipid bilayers (DOPC/DOPS/TR-PE) were introduced into the square-shaped areas surrounded by the polymeric bilayers of DiynePC (Figure 1b). Panels a and b of Figure 3 show fluorescence micrographs of the patterned bilayer in the flow cell before adding the peptide while the membranes are in contact with pure water. The polymerized bilayer appeared green because of the fluorescence from the electronic conjugation of the diacetylene polymer backbone, whereas the fluid membrane surface showed red fluorescence from TR-PE within the membrane.[42] The membrane fluidity in the square-shaped areas surrounded by the polymeric bilayers was confirmed using the FRAP technique (Figure S2 of the Supporting Information).

Three types of peptide solutions (i.e., hIAPP fibrils, soluble hIAPP, and rIAPP) or a buffer solution was injected onto the surface of the patterned bilayer in the flow cell. A diagnostic amyloid dye, thioflavin T,[50] was included in all solutions to observe the formation of amyloid aggregates on the membrane. In the case of hIAPP fibrils, we microscopically examined the patterned bilayer after incubation for 30 min following the injection of the fibril solution. The images of fluorescence from ThT, TR-PE, and the polymerized membrane were acquired at different wavelengths (see panels c and d of Figure 3 for ThT and TR-PE, respectively). The amyloid fibrils were distributed on the patterned bilayer with no evidence of selective affinity for the fluid or polymerized bilayers (Figure 3c,d). This is consistent with the binding behavior of hIAPP fibrils demonstrated by QCM-D (Figure 2a).

We obtained some intriguing results when a solution of soluble hIAPP with 5 μM ThT (no buffer components) was injected onto the patterned bilayer and the membrane was examined after incubation for 90 min. Although the fluid bilayers were visible via examination of TR-PE fluorescence, the fluorescence intensity decreased considerably upon injection of soluble hIAPP (Figure 3f). Importantly, ThT fluorescence was undetectable under the conditions employed (Figure 3e). To trigger amyloid aggregation, the standard buffer was injected onto the patterned membrane and the membrane was examined again after incubation for 30 min. ThT staining was clearly visible in the square-shaped areas (Figure 3g). ThT fluorescence intensity was comparable to that observed for hIAPP fibrils in Figure 3c, while TR-PE fluorescence was slightly enhanced after the addition of the buffer (Figure 3h). The results shown in panels e and g of Figure 3 suggest that amyloid aggregation was induced from the membrane-bound hIAPP in the fluid bilayer domains of the patterned bilayer after mixing with the buffer components.

In the nonamyloidogenic rIAPP experiment, the procedure was the same as that for soluble hIAPP. After the addition of soluble rIAPP followed by the buffer injection, ThT staining was undetectable (Figure 3i). Interestingly, after the addition of the buffer, we observed some surface irregularities in the square-shaped areas, as shown by TR-PE fluorescence (Figure 3j); the phenomenon is examined in more detail below.

FRAP Experiments. To evaluate the changes in membrane fluidity after peptide binding, we performed FRAP measurements, in which homogeneous SPBs without patterned polymeric bilayers were used. In the image shown in Figure 4a, the left-hand area is photobleached to determine the lateral diffusion coefficient of TR-PE molecules within the bilayer (see below). Subsequently, soluble hIAPP was injected onto the bilayer under the microscope. After incubation for 90 min, a

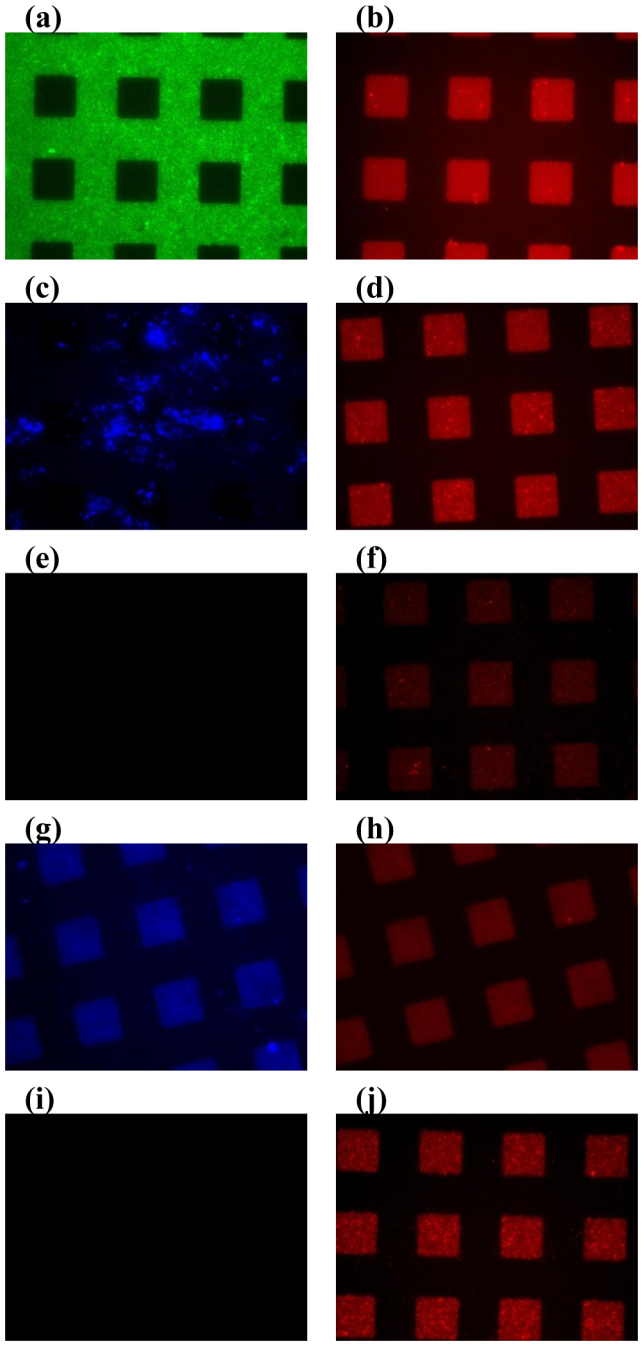

Figure 3. Binding of 7 μM IAPP to the patterned membranes. (a and b) Fluorescence micrographs of the patterned bilayer on a glass substrate. (a) Green fluorescence from the bilayer of polymerized DiynePC. (b) Red fluorescence from TR-PE within DOPC/DOPS bilayers incorporated in the corrals surrounded by the polymerized bilayer. (c and d) Fluorescence micrographs of the patterned bilayer after the addition of the hIAPP fibril solution. (c) Blue fluorescence from ThT. (d) Red fluorescence from TR-PE. (e–h) Fluorescence micrographs of the patterned bilayer after the addition of soluble hIAPP and buffer. (e and f) ThT fluorescence (nondetectable) (e) and TR-PE fluorescence (f) after addition of soluble hIAPP. (g and h) ThT fluorescence (g) and TR-PE fluorescence (h) after addition of buffer following the addition of hIAPP. (i and j) Fluorescence micrographs of the patterned bilayer after the addition of soluble rIAPP and buffer. (i) ThT fluorescence (nondetectable) and (j) TR-PE fluorescence after addition of buffer following the addition of rIAPP. The size of corrals is 20 μm × 20 μm. All images were obtained using the same illumination and processing.

dx.doi.org/10.1021/bi300542g | *Biochemistry* 2012, 51, 6908–6919

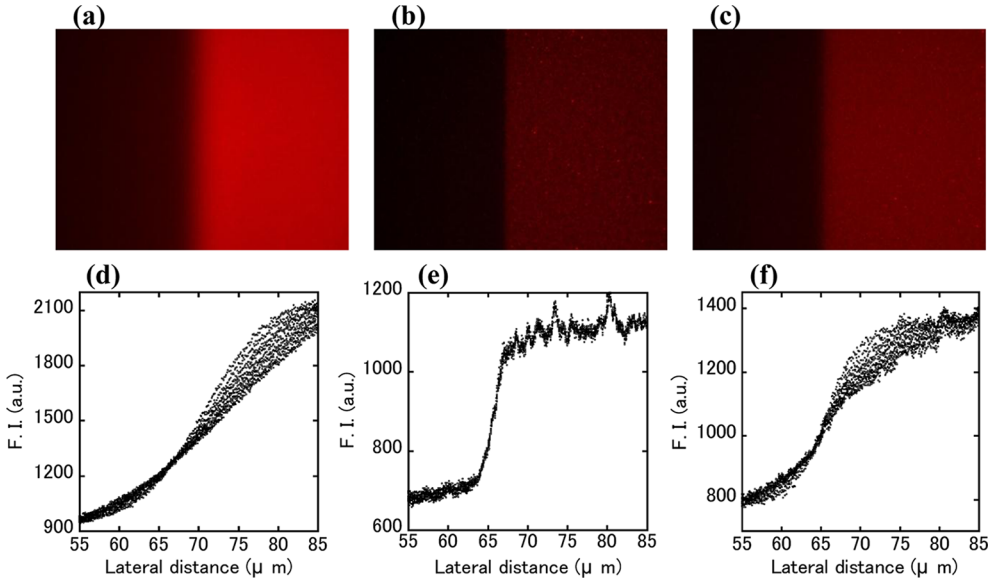

Figure 4. Changes in membrane state and fluidity upon addition of soluble hIAPP. (a–c) Fluorescence micrographs of the bilayer on a glass substrate. The images were taken just after photobleaching (left-hand areas) and before and after the addition of soluble hIAPP. (a) A TR-PE fluorescence image of the lipid bilayer. (b and c) Images of the bilayer after the addition of soluble hIAPP (b) and buffer (c). (d–f) FRAP data obtained for the samples in panels a–c, respectively. Each trace was measured every 5 s (d) or 15 s (e and f). The sizes of the images are approximately 140 μm × 100 μm.

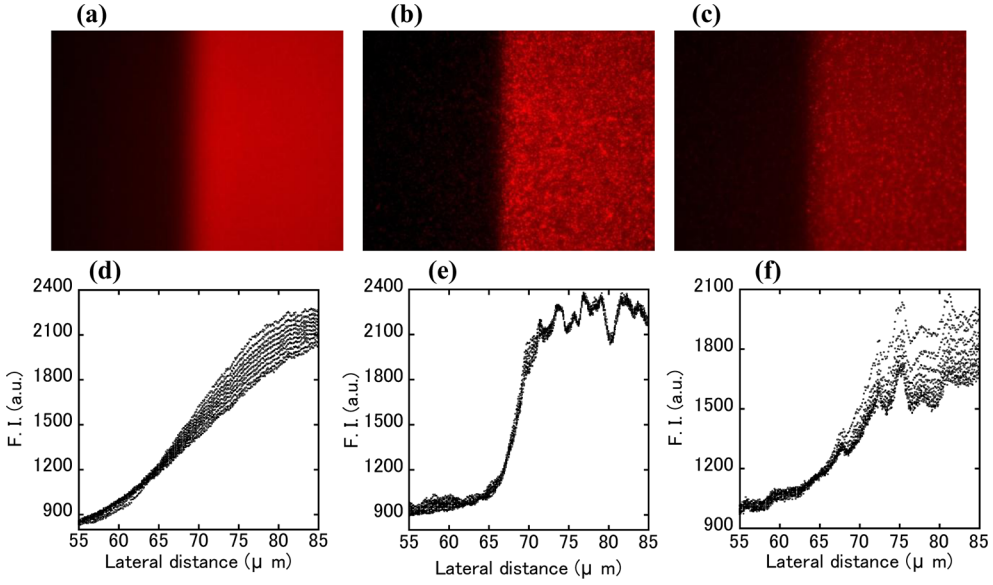

Figure 5. Changes in membrane state and fluidity upon the addition of soluble rIAPP. (a) A TR-PE fluorescence image of the lipid bilayer. (b and c) Images of the bilayer after the addition of soluble rIAPP (b) and buffer (c). (d–f) FRAP data for the samples in panels a–c, respectively.

nonbleached area was selected on the peptide-bound SPB for FRAP measurements (Figure 4b). The fluorescence intensity decreased after peptide addition (right-hand area in Figure 4b). Then, the buffer was injected onto the peptide-bound SPB to trigger amyloid aggregation at the bilayer. The sample was examined after incubation for 30 min followed by photobleaching of different parts of SPB (Figure 4c). Interestingly, the TR-PE fluorescence intensity recovered to some extent after the addition of the buffer (right-hand area in Figure 4c), which is consistent with the behavior of TR-PE fluorescence in panels f and h of Figure 3.

Figure 4d–f shows the fluorescence recovery profiles for the boundary region between the bleached and unbleached areas, plotted for successive images acquired after photobleaching (panels d–f correspond to the samples in panels a–c, respectively). The representative data of FRAP experiments, performed three times at different spots of each SPB, are presented in Figure 4. The average diffusion coefficient for the bilayer was 1.07 ± 0.20 $\mu m^2/s$ (Figure 4d). Taking into account different experimental factors, such as lipid species and the type of substrate, this value agrees with the previous result (i.e., 1.3–2.7 $\mu m^2/s$) reported for lipid bilayers on a substrate.[44,46] The diffusion coefficient became almost zero (0.004 ± 0.004 $\mu m^2/s$) after the binding of soluble hIAPP (Figure 4e). Intriguingly, after the addition of the buffer, membrane fluidity partially

dx.doi.org/10.1021/bi300542g | *Biochemistry* 2012, 51, 6908–6919

recovered (0.20 ± 0.10 $\mu m^2/s$) as did the TR-PE fluorescence intensity (Figure 4f).

Aggregation of hIAPP on SPB was visualized from its membrane-bound state under the same solution conditions as in the FRAP experiment in Figure 4b, in which two kinds of buffer solutions at pH 7.2 and 5.0 containing ThT (5 μM) were added to induce aggregation on the membrane (Figure S3 of the Supporting Information). The fluorescence images of ThT were acquired during incubation after the addition of the buffer solutions. These observations indicated that hIAPP aggregates self-assemble on the membrane during the prolonged incubation, which might be affected by the membrane fluidity as observed in Figure 4f (Figure S3 of the Supporting Information).

The experiments were repeated using soluble rIAPP at 7 μM. Fluorescence imaging after peptide addition showed drastic changes in surface morphology (Figure 5a,b). The injection of buffer onto the membrane-bound rIAPP induced a partial removal of the bilayer from the surface, resulting in extensive membrane defects and weaker fluorescence (Figure 5c). Membrane fluidity was evaluated for respective samples of rIAPP (Figure 5d–f). After the binding of soluble rIAPP, the lateral diffusion coefficient decreased (0.06 ± 0.05 $\mu m^2/s$) compared with the value (1.10 ± 0.20 $\mu m^2/s$) calculated for the intact bilayer (Figure 5d,e). Drastic changes in the surface morphology caused by the addition of the buffer to the membrane-bound rIAPP resulted in irregular boundary profiles, which hampered the determination of the diffusion coefficient (Figure 5f).

Binding of hIAPP Amyloid Fibrils to Lipid Vesicles. In our previous work, we measured turbidity to investigate the kinetics of binding between hIAPP amyloid fibrils and lipid vesicles of egg yolk phosphatidylcholine and found that these vesicles bind specifically to the fibrils.[51] In contrast, this study of SPBs showed no noticeable affinity of hIAPP amyloid fibrils for DOPC/DOPS membranes (Figures 2a and 3c). On the basis of these results, we assumed that employing entities with different morphological features, such as vesicles, might affect the affinity of fibrillar hIAPP for membranes. To examine this assumption, we investigated the binding of hIAPP fibrils to the lipid vesicles formed from DOPS or DOPC by the time-dependent changes in solution turbidity using the previously described method.[51] The hIAPP fibril solutions at various concentrations were added to DOPS vesicles, and the turbidity at 600 nm (Abs_{600}) was recorded (Figure 6a). The time-dependent turbidity of the mixture significantly increased with increasing concentrations of the fibrils (lines 2–7) compared with that of the vesicle solution without the fibrils (line 1). Abs_{600} values measured 40 s, 1 h, and 24 h after mixing were plotted after subtraction of the values for the vesicle components versus the concentration of the fibrils (Figure 6b). The plots showed a linear dependence of solution turbidity on fibril concentration.

We repeated the experiment using DOPC vesicles (Figure S4 of the Supporting Information) and prepared a similar plot for the resultant Abs_{600} values, again showing a linear dependence of Abs_{600} values on the fibril concentration (Figure 6c). This binding behavior is very similar to the binding between hIAPP fibrils and vesicles formed form egg yolk phosphatidylcholine.[51] As reported previously,[51] these results demonstrate the binding of the vesicles to the surface of amyloid fibrils, the extent of which is enhanced in direct proportion to the concentration of hIAPP fibrils (in the presence of excess vesicles).

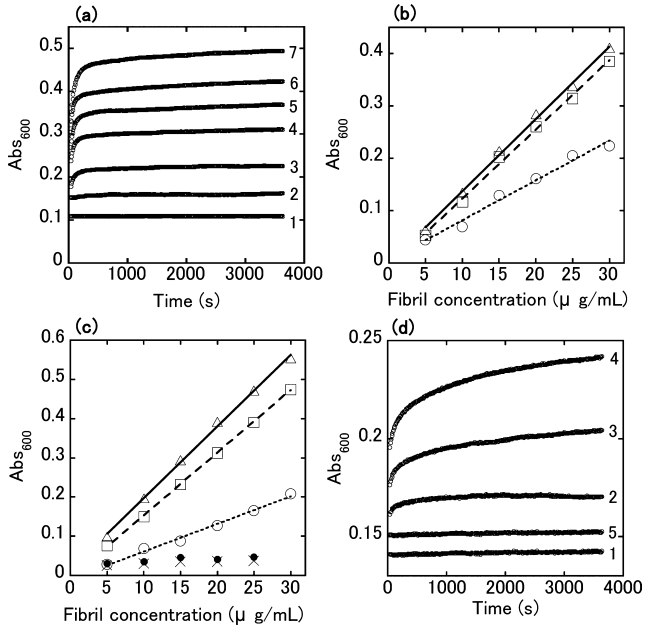

Figure 6. Effect of hIAPP fibril concentration on binding with lipid vesicles at 25 °C and pH 7.2. (a) Time-dependent changes in the apparent solution absorbance (Abs_{600}) for hIAPP fibrils at various concentrations (0–30 μg/mL) and DOPS vesicles (3.0 mg/mL). Fibril concentrations were 0 (1), 5 (2), 10 (3), 15 (4), 20 (5), 25 (6), and 30 μg/mL (7), from bottom to top, respectively. (b and c) Abs_{600} measured 40 s, 1 h, and 24 h after mixing. (b) The Abs_{600} values for the samples in panel a were plotted (after subtraction of Abs_{600} for the vesicle components) vs the concentration of hIAPP fibrils: after 40 s (○), 1 h (□), and 24 h (△). (c) Similarly, the Abs_{600} values were plotted for the samples containing the DOPC or DMPC vesicles: after 40 s (○), 1 h (□), and 24 h (△) for DOPC vesicles and after 1 h (×) and 24 h (●) for DMPC vesicles. Panels b and c show the linear best fits to the respective marks. (d) Time-dependent values of Abs_{600} for buffer-induced hIAPP fibrils and DOPS/DOPC vesicles. Fibrillation was induced by mixing the aqueous solution containing dissolved hIAPP and dispersed vesicles with the buffer solution at the different final concentrations: buffer-free (1), 0.5 mM phosphate and 1 mM NaCl buffer (2), 1.7 mM phosphate and 3.4 mM NaCl buffer (3), and 5 mM phosphate and 10 mM NaCl buffer (4). Line 5 represents the time dependence of Abs_{600} for the rIAPP sample under the same conditions as in the experiment represented by line 4. The concentrations of IAPP and vesicles were 30 μg/mL and 3.0 mg/mL, respectively.

To obtain additional information about the effect of lipid type on the binding reaction, we used the vesicles formed from dimyristoylphosphatidylcholine (DMPC), which has shorter hydrophobic alkyl chains and a higher gel–liquid crystalline-phase transition (23 °C) than DOPC (−20 °C). We observed the time-dependent changes in Abs_{600} values for DMPC vesicles (Figure S5 of the Supporting Information). However, the changes were much smaller than those for DOPS and DOPC vesicles, probably reflecting a weaker binding affinity of DMPC vesicles for hIAPP fibrils (Figure 6c).

We also investigated the effect of the fibrillation state of hIAPP on the binding reaction with DOPC/DOPS (4/1) vesicles using a modified turbidity assay. First, a 0.4 mg/mL solution of soluble hIAPP in water and DMSO (see Materials and Methods) was mixed with DOPC/DOPS vesicles dispersed in water. Different amounts of the standard buffer (or pure water) were added to the solution, giving solutions containing 30 μg/mL hIAPP and 3.0 mg/mL DOPC/DOPS vesicles and

dx.doi.org/10.1021/bi300542g | Biochemistry 2012, 51, 6908–6919

buffer components at several concentrations (0−15 mM). We measured solution turbidity immediately after mixing. The buffer-free solution showed no noticeable increase in Abs_{600} values (line 1 in Figure 6d). However, the turbidity value increased with increasing amounts of buffer (lines 2−4 in Figure 6d). We also confirmed the adsorption of soluble hIAPP to the lipid vesicles in the absence of the buffer components (Figure S6 of the Supporting Information).

To determine whether the increase in Abs_{600} values corresponds to an increase in the level of amyloid fibril formation, we conducted the ThT fluorescence assay for samples 1−4 shown in Figure 6d immediately after turbidity had been recorded. The results showed enhanced ThT fluorescence for the samples with increased buffer content (Figure S7 of the Supporting Information), confirming that the accelerated turbidity changes observed in Figure 6d can be attributed to the increased level of buffer-induced amyloid fibril formation. The modified turbidity assay was also conducted for soluble rIAPP. No noticeable increase in Abs_{600} values was observed in the presence of the buffer components (line 5 in Figure 6d).

DISCUSSION

Binding of Soluble IAPP to SPBs. As shown in Figure 2b, soluble hIAPP exhibits a pronounced ability to bind to SPB, as demonstrated by the decrease in the oscillation frequency, f, and its distinctive asymptotic curve. The addition of buffer at the membrane-bound stage triggers amyloid aggregation at the membrane (Figure 3g and Figure S3 of the Supporting Information) and causes a further decrease in the oscillation frequency. The membrane binding of hIAPP and subsequent buffer addition are accompanied by the increase in dissipation, D, as a result of the changes in the viscoelastic and frictional properties of the adsorbing surface (Figure 2b). As the mechanically coupled mass measured by QCM-D also reflects the mass of water involved in the reactions at the membrane, the decrease in f values associated with amyloid aggregation suggests that water molecules might be trapped inside or between the amyloid aggregates.[52]

In contrast, soluble rIAPP exhibits the membrane binding behavior lacking marked asymptotic traces (Figure 2c). Interestingly, a slight increase in f was observed upon the addition of buffer to rIAPP in the membrane-bound state; the final Δf value (~25 Hz) was smaller than the value (~28 Hz) detected for the bilayer formation under identical conditions (Figure 2c). This result implies that some lipid components were extracted from the bilayer on the sensor, which was verified by fluorescence imaging (Figures 3j and 5c,f).

hIAPP and rIAPP carry three positive charges at the N-terminal region at neutral pH (N-terminus, K1, and R11). Adsorption of soluble hIAPP and rIAPP onto negatively charged lipid membranes has been also studied by other authors. The reported results demonstrate that the positively charged N-terminus is responsible for the insertion of IAPP into negatively charged lipid membranes mainly via electrostatic interactions.[13,53,54] Both hIAPP and rIAPP form a transient α-helical structure after membrane binding. In the case of hIAPP, in this structure, the N-terminal region (residues 1−22) takes part in secondary structure formation whereas the C-terminal region (residues 23−37) remains in the disordered state.[13,14,54−56]

The results of this study reveal very different levels of peptide−membrane interactions for the two IAPP species, as demonstrated by the QCM measurements (Figure 2) and microscopic observation (Figures 3−5). In particular, it is noteworthy that the binding behavior of the soluble hIAPP is associated with a much larger decrease in the oscillation frequency than the changes observed for rIAPP. Thus, the data indicate that additional factors other than the electrostatic interactions play an important role in determining the mode of hIAPP−SPB binding.

Recent studies of membrane interactions of rat and human $IAPP_{1-19}$ fragments (residues 1−19, with a substitution of arginine for histidine at residue 18) with dodecylphosphocholine detergent micelles show that $hIAPP_{1-19}$ is buried deep within the micelles while $rIAPP_{1-19}$ is located at the micelle surface, although both peptides fold into similar helical conformations.[56,57] The authors have suggested that deprotonation of H18 in hIAPP is important for its orientation while binding to the micelle surface. In this regard, we observed the membrane-mediated aggregation of hIAPP from its membrane-bound state by adding the different buffer solutions at pH 7.2 and 5.0 (Figure S3 of the Supporting Information). The result showed that the solution condition at pH 7.2 tends to promote aggregation in the initial stages of incubation. Thus, it is possible that deprotonation of H18 has a bearing on the QCM-D data for the two full-length peptides obtained in our study, but the extent of the contribution is unclear.

Recently, Rosa and colleagues have studied membrane interactions of an amyloidogenic peptide with the sequence corresponding to the 12−18 N-terminal regions of hIAPP and its variants.[58] Their results suggest that complex factors, such as size and hydrophobic and/or electrostatic character of the side chain and β-sheet propensity, act synergistically to affect interpeptide aggregation and peptide−membrane interactions. In light of the binding characteristics of IAPP reported previously,[13,14,53−58] we infer that the marked membrane affinity of soluble hIAPP observed in Figure 2b can be attributed to the conversion of the peptide into membrane-associated secondary structure (α-helical structure), occurring deep within the bilayer, whereas rIAPP adopts the secondary structure partly at the membrane surface. We presume that the addition of buffer (Figure 2c, mark 4) alters the balance of electrostatic and hydrophobic factors affecting the lipid−rIAPP aggregates, partially detaching the aggregates from the bilayer surface (Figure 5c,f).

Amyloid Aggregation on the Micropatterned Model Membranes. The peptide sequence within residues 20−29 of hIAPP is considered to be a highly amyloidogenic region.[25] This region also exhibits the largest sequence variations between IAPP species.[59] It has been reported that the formation of α-helical, membrane-bound hIAPP exposes a highly amyloidogenic stretch of residues 20−29 to an aqueous environment. This exposure promotes amyloid aggregation by the combined effects of the increased local concentration, the enhanced orientation of the peptide, and the low-dielectric environment near the membrane.[14,55] Thus, the α-helical, membrane-bound oligomeric states have been suggested as possible intermediates in the amyloid aggregation of hIAPP at lipid membranes, but their topology and stoichiometry remain elusive.[13,14,54−56]

In this study, we demonstrate amyloid aggregation of soluble hIAPP at the square-shaped areas of fluid bilayers of the patterned membrane (Figure 3g) and the growth of aggregates on homogeneous SPB (Figure S3 of the Supporting Information). These observations have important implications

for the membrane-mediated aggregation following the penetration of soluble hIAPP into the fluid membranes. Recently, it has been reported that elongation of hIAPP fibrils at the membrane, but not the fibrils themselves, could cause membrane disruption, possibly by increasing the membrane curvature or by the incorporation of lipid into the growing fibrils.[60] Furthermore, it has been proposed that membrane composition is a key factor in regulating hIAPP aggregation on lipid membranes.[61] Chemical analyses of fibrillar deposits found in tissues in a number of amyloid diseases suggest that lipid constituents of cells can be incorporated into the growing fibrils.[62] Therefore, it seems reasonable to postulate that amyloid aggregation of the membrane-bound forms of hIAPP damages the membrane structure by incorporating the lipid components into the forming aggregates in a membrane composition-dependent manner.[60−63]

Changes in Membrane Fluidity and Morphology. The fluidity of lipid bilayers is critical to biological functions in cell membranes. Formation of lipid microdomains (e.g., lipid rafts) and assembly of membrane proteins into signaling complexes are influenced by the lateral mobility of lipid membranes.[64] The diffusion measurements have been widely applied to characterize lipid mobility for both model lipid bilayers and cell membranes.[44,46,65−69] In this study, we quantitatively evaluated, using FRAP measurements, the effects of membrane binding and amyloid aggregation of IAPP on lateral diffusion of TR-PE within the bilayer (Figures 4 and 5). The diffusion coefficient decreases substantially after the membrane binding of soluble hIAPP and rIAPP, with hIAPP species being more effective under the same conditions. As the extent of reduction in the membrane fluidity depends on the nature of interactions between obstacles (e.g., membrane-bound peptide) and diffusing lipid molecules,[44,68,69] the decrease in the extent of lateral diffusion presented in Figure 4e can be attributed to various factors, including the amount, location, and conformation of membrane-bound IAPP.

In the case of hIAPP, the membrane fluidity recovers to some degree after the buffer is added to induce amyloid aggregation (Figure 4f), and a partial recovery of the TR-PE fluorescence intensity is also observed (Figure 4c). As the change from water to buffer did not affect significantly the membrane fluidity of the bilayer (data not shown), this recovery suggests that membrane fluidity is affected by the hIAPP binding process and amyloid aggregation in the membrane-bound state. The decrease in TR-PE fluorescence intensity upon hIAPP binding might be ascribed to the self-quenching caused by the increase in the local concentration of negatively charged TR-PE associated with hIAPP molecules (Figure 4b). Considering the possibility of specific interactions between TR-PE and hIAPP, it could be argued that it is the lateral mobility of TR-PE, and not the whole membrane fluidity, that is mostly affected. Although the extent of this effect is not clear, we suggest that after the majority of lipids are released from hIAPP-bound forms upon buffer-induced aggregation of the peptide, some of the lipid molecules are attracted or incorporated into the aggregates. This might explain the fact that the membrane fluidity recovers only partly (Figure 4c,f). The effect of fluorescence resonance energy transfer between TR-PE and ThT should be small as we observed similar changes in TR-PE fluorescence before and after the additions of soluble hIAPP and buffer in Figures 3 and 4 (ThT was not used in the experiments shown in Figure 4).

When nonamyloidogenic rIAPP binds to the bilayer, small irregular aggregates containing fluorescent lipids appear on the surface (Figure 5b). As we observed that some lipids detach themselves from the bilayer after buffer injection, we believe that the aggregates might contain a substantial amount of lipids (Figure 5c). This finding indicates the ability of rIAPP to associate with the lipid membrane under the conditions that are used. However, if we take into account that rIAPP is much less toxic to β-cells than hIAPP,[12,21−23] this association property probably does not cause significant damage to the cell membrane. In contrast, the cytotoxicity of hIAPP presumably stems from its various abilities to perturb lipid membranes, as discussed below.

Membrane Affinity of Fibrillar hIAPP. As shown in Figure 6a−c, the solution turbidity representing the binding between hIAPP fibrils and DOPS or DOPC vesicles is significantly enhanced by increasing the amount of hIAPP fibrils. In the initial stages (0−1000 s) of the incubation with hIAPP fibrils, the increase in Abs_{600} is much more rapid for DOPS vesicles than for DOPC vesicles, indicating the electrostatic effect accelerating the initial binding process. Although the DMPC vesicles also bind hIAPP fibrils, the level of binding is much lower, as judged by the results of turbidity measurements. We can conclude that the extent of binding depends on the physicochemical properties of vesicles, such as the different hydrophobic nature and phase transition behavior of the lipids.

Intriguingly, the QCM-D experiments (Figure 2) showed that the binding affinity of fibrillar hIAPP for SPB consisting of DOPC and DOPS is very low under the same conditions that were used in the turbidity assay. The differences between the affinity of hIAPP fibrils for the vesicles and SPB may be ascribed to their different diffusion behaviors. Small vesicles (~100 nm) can move freely in solutions and frequently collide with the fibrils; the fibrils are large (several micrometers), and their diffusion toward the immobile SPB can be slow. The membrane binding of hIAPP fibrils may also be affected by other complex factors, such as lipid type and structural differences between vesicles and SPBs (e.g., critical packing parameter).

Potential Roles of Oligomeric hIAPP in Membrane Dysfunction. There is a growing body of evidence supporting the hypothesis that amyloid oligomers, rather than the mature amyloid fibrils themselves, are the primary cell-toxic species.[27−29] Furthermore, the common structure of various amyloid oligomers suggests a common mechanism of cytotoxicity.[70] Therefore, it is important to clarify how toxic amyloid oligomers interact with cellular membranes and induce cell death. As membrane damage caused by amyloidogenic peptides under physiological conditions is a complex process in which multiple oligomeric states are involved in a membrane composition-dependent manner,[15−20,60−63] it is not likely that a single common mechanism is solely responsible for the amyloid-induced cytotoxicity of a given amyloidogenic polypeptide.[71]

As shown in Figure 4a−f, the FRAP data obtained in this study using model membranes demonstrate that the adsorption of soluble hIAPP to SPBs causes a significant reduction in the membrane fluidity, which is crucial to various cellular functions.[64−69] We also demonstrate amyloid aggregation of hIAPP at the fluid lipid domains of the patterned membrane (Figure 3g) and the time-dependent assembly of the aggregates (Figure S3 of the Supporting Information). Amyloid

aggregation of the membrane-bound hIAPP could result in membrane damage by incorporation of lipids into the growing aggregates.[60,62,63] Moreover, the results of the fibril-mediated aggregation of the lipid vesicles (Figure 6) show that the fibrillar hIAPP forms (including their initial states) might have a lateral ability to perturb the membrane structure. These results suggest that membrane-bound forms of hIAPP might be the species that effectively exert toxic effects on cells; they can affect the membrane fluidity, grow into larger fibrillar (or oligomeric) forms in the membrane-bound state, and perturb lipid components by attracting them (Figure 7a,b). In vivo, such

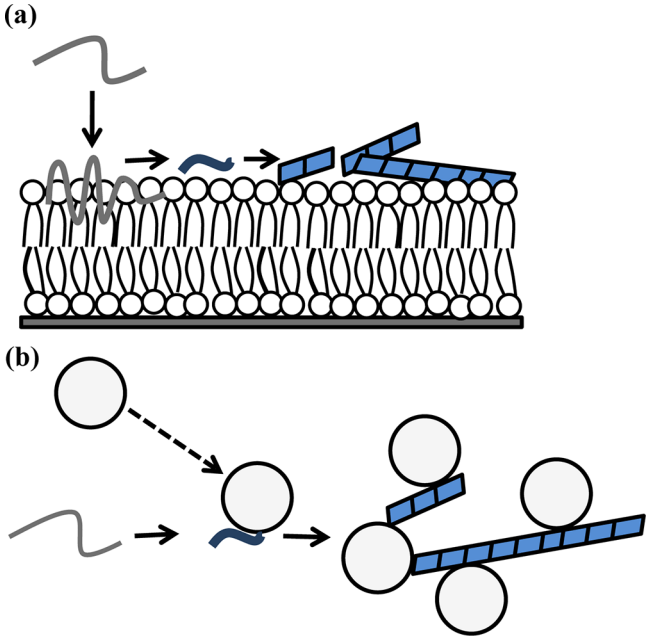

Figure 7. Simplified schematic representation of interactions of amyloidogenic hIAPP with SPBs and lipid vesicles. (a) Adsorption or insertion of soluble hIAPP either as a monomer or as an oligomer on the surface of the membrane or into the membrane causes a substantial decrease in membrane fluidity. Amyloid aggregation of the membrane-bound hIAPP could result in membrane damage by extracting the lipids and incorporating them into the aggregates. (b) Binding between lipid vesicles and hIAPP in the fibrillar state leads to fibril–lipid association (aggregation).

toxic effects of hIAPP are now postulated to be strictly regulated by insulin that is secreted with the peptide, in the process where the molar ratio of hIAPP to insulin is maintained at about 1:100 in healthy β-cells and changes substantially (to 1:20) in diseased cells.[1,6,72,73]

■ ASSOCIATED CONTENT

Supporting Information

Binding behavior of IAPP at 5 μM (Figure S1), membrane fluidity of the patterned bilayer (Figure S2), aggregation of hIAPP on PBS (Figure S3), turbidity measurements for DOPC vesicle–hIAPP fibrils (Figure S4) and DMPC vesicle–hIAPP fibrils (Figure S5), analysis of vesicle–hIAPP binding (Figure S6), and a ThT fluorescence assay (Figure S7). This material is available free of charge via the Internet at http://pubs.acs.org.

■ AUTHOR INFORMATION

Corresponding Author

*E-mail: sasahara@med.kobe-u.ac.jp. Telephone: +81-78-382-5701. Fax: +81-78-382-5701.

Funding

This research was supported by grants from Global COE program A08 from the Ministry of Education, Culture, Sports, Science and Technology of Japan (to D.H. and K.S.).

Notes

The authors declare no competing financial interest.

■ ACKNOWLEDGMENTS

We thank Ms. Saori Mori (AIST) for her assistance in the experiments.

■ ABBREVIATIONS

hIAPP, human islet amyloid polypeptide; rIAPP, rat islet amyloid polypeptide; T2DM, type II diabetes mellitus; SPB, substrate-supported planar bilayer; DiynePC, diacetylene phospholipid [1,2-bis(10,12-tricosadiynoyl)-*sn*-glycero-3-phosphocholine]; DOPC, 1,2-dioleoyl-*sn*-glycero-3-phosphocholine; DOPS, 1,2-dioleoyl-*sn*-glycero-3-phospho-L-serine; DMPC, 1,2-dimyristoyl-*sn*-glycero-3-phosphocholine; TR-PE, Texas Red 1,2-dihexadecanoyl-*sn*-glycerophosphoethanolamine; QCM-D, quartz crystal microbalance with dissipation monitoring; FRAP, fluorescence recovery after photobleaching; DMSO, dimethyl sulfoxide; SDS, sodium dodecyl sulfate; ThT, thioflavin T.

■ REFERENCES

(1) Hull, R. L., Westermark, G. T., Westermark, P., and Kahn, S. E. (2004) Islet amyloid: A critical entity in the pathogenesis of type 2 diabetes. *J. Clin. Endocrinol. Metab. 89*, 3629–3643.

(2) Höppener, J. W. M., and Lips, C. J. M. (2006) Role of islet amyloid in type 2 diabetes mellitus. *Int. J. Biochem. Cell Biol. 38*, 726–736.

(3) Haataja, L., Gurlo, T., Huang, C. J., and Butler, P. C. (2008) Islet amyloid in type 2 diabetes, and the toxic oligomer hypothesis. *Endocr. Rev. 29*, 303–316.

(4) Jaikaran, E. T. A. S., and Clark, A. (2001) Islet amyloid and type 2 diabetes: From molecular misfolding to islet pathophysiology. *Biochim. Biophys. Acta 1537*, 179–203.

(5) Clark, A., and Nilsson, M. R. (2004) Islet amyloid: A complication of islet dysfunction or an aetiological factor in Type 2 diabetes? *Diabetologia 47*, 157–169.

(6) Kahn, S. E., D'Alessio, D. A., Schwartz, M. W., Fujimoto, W. Y., Ensinck, J. W., Taborsky, G. J., Jr., and Porte, D., Jr. (1990) Evidence of cosecretion of islet amyloid polypeptide and insulin by β-cells. *Diabetes 39*, 634–638.

(7) Gedulin, B. R., Jodka, C. M., Herrmann, K., and Young, A. A. (2006) Role of endogenous amylin in glucagon secretion and gastric emptying in rats demonstrated with the selective antagonist, AC187. *Regul. Pept. 137*, 121–127.

(8) Akesson, B., Panagiotidis, G., Westermark, P., and Lundquist, I. (2003) Islet amyloid polypeptide inhibits glucagon release and exerts a dual action on insulin release from isolated islets. *Regul. Pept. 111*, 55–60.

(9) Chiti, F., and Dobson, C. M. (2006) Protein misfolding, functional amyloid, and human disease. *Annu. Rev. Biochem. 75*, 333–366.

(10) Padrick, S. B., and Miranker, A. D. (2001) Islet amyloid polypeptide: Identification of long-range contacts and local order on the fibrillogenesis pathway. *J. Mol. Biol. 308*, 783–794.

(11) Knight, J. D., and Miranker, A. D. (2004) Phospholipid catalysis of diabetic amyloid assembly. *J. Mol. Biol. 341*, 1175–1187.

(12) Jayasinghe, S. A., and Langen, R. (2005) Lipid membranes modulate the structure of islet amyloid polypeptide. *Biochemistry 44*, 12113−12119.
(13) Lopes, D. H. J., Meister, A., Gohlke, A., Hauserm, A., Blume, A., and Winter, R. (2007) Mechanism of islet amyloid polypeptide fibrillation at lipid interfaces studied by infrared reflection absorption spectroscopy. *Biophys. J. 93*, 3132−3141.
(14) Williamson, J. A., Loria, J. P., and Miranker, A. D. (2009) Helix stabilization precedes aqueous and bilayer-catalyzed fiber formation in islet amyloid polypeptide. *J. Mol. Biol. 393*, 383−396.
(15) Janson, J., Ashley, R. H., Harrison, D., McIntyre, S., and Butler, P. C. (1999) The mechanism of islet amyloid polypeptide toxicity is membrane disruption by intermediate-sized toxic amyloid particles. *Diabetes 48*, 491−498.
(16) Anguiano, M., Nowak, R. J., and Lansbury, P. T., Jr (2002) .Protofibrillar islet amyloid polypeptide permeabilizes synthetic vesicles by a pore-like mechanism that may be relevant to type II diabetes. *Biochemistry 41*, 11338−11343.
(17) Porat, Y., Kolusheva, S., Jelinek, R., and Gazit, E. (2003) The human islet amyloid polypeptide forms transient membrane-active prefibrillar assemblies. *Biochemistry 42*, 10971−10977.
(18) Kayed, R., Sokolov, Y., Edmonds, B., McIntire, T. M., Milton, S. C., Hall, J. E., and Glabe, C. G. (2004) Permeabilization of lipid bilayers is a common conformation-dependent activity of soluble amyloid oligomers in protein misfolding diseases. *J. Biol. Chem. 279*, 46363−46366.
(19) Demuro, A., Mina, E., Kayed, R., Milton, S. C., Parker, I., and Glabe, C. G. (2005) Calcium dysregulation and membrane disruption as a ubiquitous neurotoxic mechanism of soluble amyloid oligomers. *J. Biol. Chem. 280*, 17294−17300.
(20) Ritzel, R. A., Meier, J. J., Lin, C.-Y., Veldhuis, J. D., and Butler, P. C. (2007) Humann islet amyloid polypeptide oligomers disrupt cell coupling, induce apoptosis, and impair insulin secretion in isolated human islets. *Diabetes 56*, 65−71.
(21) Westermark, P., Engström, U., Johnson, K. H., and Westermark, G. T. (1990) Islet amyloid polypeptide: Pinpointing amino acid residues linked to amyloid fibril formation. *Proc. Natl. Acad. Sci. U.S.A. 87*, 5036−5040.
(22) Knight, J. D., Hebda, J. A., and Miranker, A. D. (2006) Conserved and cooperative assembly of membrane-bound α-helical states of islet amyloid polypeptide. *Biochemistry 45*, 9496−9508.
(23) Lin, C.-Y., Gurlo, T., Kayed, R., Butler, A. E., Haataja, L., Glabe, C. G., and Butler, P. C. (2007) Toxic human islet amyloid polypeptide (h-IAPP) oligomers are intracellular, and vaccination to induce anti-toxic oligomer antibodies does not prevent h-IAPP-induced β-cell apoptosis in h-IAPP transgenic mice. *Diabetes 56*, 1324−1332.
(24) Matveyenko, A. V., and Butler, P. C. (2006) Islet amyloid polypeptide (IAPP) transgenic rodents as models for type 2 diabetes. *ILAR J. 47*, 225−233.
(25) Jayasinghe, S. A., and Langen, R. (2007) Membrane interaction of islet amyloid polypeptide. *Biochim. Biophys. Acta 1768*, 2002−2009.
(26) Engel, M. F. M. (2009) Membrane permeabilization by islet amyloid polypeptide. *Chem. Phys. Lipids 160*, 1−10.
(27) Quist, A., Doudevski, I., Lin, H., Azimova, R., Ng, D., Frangione, B., Kagan, B., Ghiso, J., and Lal, R. (2005) Amyloid ion channels: A common structural link for protein-misfolding disease. *Proc. Natl. Acad. Sci. U.S.A. 102*, 10427−10432.
(28) Lashuel, H. A., and Lansbury, P. T. (2006) Are amyloid diseases caused by protein aggregates that mimic bacterial pore-forming toxins? *Q. Rev. Biophys. 39*, 167−201.
(29) Glabe, C. G., and Kayed, R. (2006) Common structure and toxic function of amyloid oligomers implies a common mechanism of pathogenesis. *Neurology 66*, S74−S78.
(30) Huang, C.-j., Lin, C.-y., Haataja, L., Gurlo, T., Butler, A. E., Rizza, R. A., and Butler, P. C. (2007) High expression rates of human islet amyloid polypeptide induce endoplasmic reticulum stress-mediated β-cell apoptosis, a characteristic of humans with type 2 but not type 1 diabetes. *Diabetes 56*, 2016−2027.
(31) Lupi, R., and Del Prato, S. (2008) β-Cell apoptosis in type 2 diabetes: Quantitative and functional consequences. *Diabetes Metab. 34*, S56−S64.
(32) Hoffstrom, B. G., Kaplan, A., Letso, R., Schmid, R. S., Turmel, G. J., Lo, D. C., and Stockwell, B. R. (2010) Inhibitors of protein disulfide isomerase suppress apoptosis induced by misfolded proteins. *Nat. Chem. Biol. 6*, 900−906.
(33) Cho, W.-J., Trikha, S., and Jeremic, A. M. (2009) Cholesterol regulates assembly of human islet amyloid polypeptide on model membranes. *J. Mol. Biol. 393*, 765−775.
(34) Scalisi, S., Sciacca, M. F. M., Zhavnerko, G., Grasso, D. M., Marletta, G., and La Rosa, C. (2010) Self-assembling pathway of hiapp fibrils within lipid bilayers. *ChemBioChem 11*, 1856−1859.
(35) Fu, L., Liu, J., and Yan, E. C. Y. (2011) Chiral sum frequency generation spectroscopy for characterizing protein secondary structures at interfaces. *J. Am. Chem. Soc. 133*, 8094−8097.
(36) Xiao, D., Fu, L., Liu, J., Batista, V. S., and Yan, E. C. Y. (2012) Amphiphilic adsorption of human islet amyloid polypeptide aggregates to lipid/aqueous interfaces. *J. Mol. Biol. 421*, 537−547.
(37) Groves, J. T., and Boxer, S. G. (2002) Micropattern formation in supported lipid membranes. *ACC Chem. Res. 35*, 149−157.
(38) Tanaka, M., and Sackmann, E. (2005) Polymer-supported membranes as models of the cell surface. *Nature 437*, 656−663.
(39) Green, J. D., Kreplak, L., Goldsbury, C., Blatter, X. L., Stolz, M., Cooper, G. S., Seelig, A., Kistler, J., and Aebi, U. (2004) Atomic force microscopy reveals defects within mica supported lipid bilayers induced by the amyloidogenic human amylin peptide. *J. Mol. Biol. 342*, 877−887.
(40) Domanov, Y. A., and Kinnunen, P. K. J. (2008) Islet amyloid polypeptide forms rigid lipid-protein amyloid fibrils on supported phospholipid bilayers. *J. Mol. Biol. 376*, 42−54.
(41) Morigaki, K., Baumgart, T., Offenhäusser, A., and Knoll, W. (2001) Patterning solid-supported lipid bilayer membranes by lithographic polymerization of a diacetylene lipid. *Angew. Chem., Int. Ed. 40*, 172−174.
(42) Morigaki, K., Kiyosue, K., and Taguchi, T. (2004) Micro-patterned composite membranes of polymerized and fluid lipid bilayers. *Langmuir 20*, 7729−7735.
(43) Morigaki, K., Schönherr, H., and Okazaki, T. (2007) Polymerization of diacetylene phospholipid bilayers on solid substrate: Influence of the film deposition temperature. *Langmuir 23*, 12254−12260.
(44) Okazaki, T., Inaba, T., Tatsu, Y., Tero, R., Urisu, T., and Morigaki, K. (2009) Polymerized lipid bilyers on a solid substrate: Morphologies and obstruction of lateral diffusion. *Langmuir 25*, 345−351.
(45) Rustenbeck, I., Matthies, A., and Lenzen, S. (1994) Lipid composition of glucose-stimulated pancreatic islets and insulin-secreting tumor cells. *Lipids 29*, 685−692.
(46) Merzlyakov, M., Li, E., and Hristova, K. (2006) Directed assembly of surface-supported bilayers with transmembrane helices. *Langmuir 22*, 1247−1253.
(47) Keller, C. A., and Kasemo, B. (1998) Surface specific kinetics of lipid vesicle adsorption measured with a quartz crystal microbalance. *Biophys. J. 75*, 1397−1402.
(48) Glasmästar, K., Larsson, C., Höök, F., and Kasemo, B. (2002) Protein adsorption on supported phospholipid bilayers. *J. Colloid Interface Sci. 246*, 40−47.
(49) Okazaki, T., Morigaki, K., and Taguchi, T. (2006) Phospholipid vesicle fusion on micropatterned polymeric bilayer substrates. *Biophys. J. 91*, 1757−1766.
(50) Levine, H., III (1999) Quantification of β-sheet amyloid fibril structures with thioflavin T. *Methods Enzymol. 309*, 274−284.
(51) Sasahara, K., Hall, D., and Hamada, D. (2010) Effect of lipid type on the binding of lipid vesicles to islet amyloid polypeptide amyloid fibrils. *Biochemistry 49*, 3040−3048.
(52) Peruz, M. F., Finch, J. T., Berriman, J., and Lesk, A. (2002) Amyloid fibers are water-filled nanotubes. *Proc. Natl. Acad. Sci. U.S.A. 99*, 5591−5595.

(53) Engel, M. F. M., Yigittop, H., Elgersma, R. C., Rijkers, D. T. S., Liskamp, R. M. J., de Kruijff, B., Höppener, J. W. M., and Killian, J. A. (2006) Islet amyloid polypeptide inserts into phospholipid monolayers as monomer. *J. Mol. Biol. 356*, 783−789.
(54) Williamson, J. A., and Miranker, A. D. (2007) Direct detection of transient α-helical states in islet amyloid polypeptide. *Protein Sci. 16*, 110−117.
(55) Apostolidou, M., Jayasinghe, S. A., and Langen, R. (2008) Structure of α-helical membrane-bound human islet amyloid polypeptide and its implications for membrane-mediated misfolding. *J. Biol. Chem. 283*, 17205−17210.
(56) Nanga, R. P. R., Brender, J. R., Xu, J., Veglia, G., and Ramamoorthy, A. (2008) Structures of rat and human islet amyloid polypeptide $IAPP_{1-19}$ in micelles by NMR spectroscopy. *Biochemistry 47*, 12689−12697.
(57) Brender, J. R., Hartman, K., Reid, K. R., Kennedy, R. T., and Ramamoorthy, A. (2008) A single mutation in the nonamyloidogenic region of islet amyloid polypeptide greatly reduces toxicity. *Biochemistry 47*, 12680−12688.
(58) Milardi, D., Sciacca, M. F. M., Pappalardo, M., Grasso, D. M., and Rosa, C. L. (2011) The role of aromatic side-chains in amyloid growth and membrane interaction of the islet amyloid polypeptide. *Eur. Biophys. J. 40*, 1−12.
(59) Moriarty, D. F., and Raleigh, D. P. (1999) Effects of sequential proline substitutions on amyloid formation by human $amylin_{20-29}$. *Biochemistry 38*, 1811−1818.
(60) Engel, M. F. M., Khemtémourian, L., Kleijer, C. C., Meeldijk, H. J. D., Jacobs, J., Verkleij, A. J., de Kruijff, B., Killian, J. A., and Höppener, J. W. M. (2008) Membrane damage by human islet amyloid polypeptide through fibril growth at the membrane. *Proc. Natl. Acad. Sci. U.S.A. 105*, 6033−6038.
(61) Trikha, S., and Jeremic, A. M. (2011) Clustering and internalization of toxic amylin oligomers in pancreatic cells require plasma membrane cholesterol. *J. Biol. Chem. 286*, 36086−36097.
(62) Gellermann, G. P., Appel, T. R., Tannert, A., Radestock, A., Hortschansky, P., Schroeckh, V., Leisner, C., Lütkepohl, T., Shtrasburg, S., Röcken, C., Pras, M., Linke, R. P., Diekmann, S., and Fändrich, M. (2005) Raft lipids as common components of human extracellular amyloid fibrils. *Proc. Natl. Acad. Sci. U.S.A. 102*, 6297−6302.
(63) Radovan, D., Opitz, N., and Winter, R. (2009) Fluorescence microscopy studies on islet amyloid polypeptide fibrillation at heterogeneous and cellular membrane interfaces and its inhibition by resveratrol. *FEBS Lett. 583*, 1439−1445.
(64) Lingwood, D., and Simon, K. (2010) Lipid rafts as a membrane-organizing principle. *Science 327*, 46−50.
(65) Winckler, B., Forscher, P., and Mellman, I. (1999) A diffuson barrier maintains distribution of membrane proteins in polarized neurns. *Nature 397*, 698−701.
(66) Kusumi, A., Nakada, C., Ritchie, K., Murase, K., Suzuki, K., Murakoshi, H., Kasai, R. S., Kondo, J., and Fujiwara, T. (2005) Paradigm shift of the plasma membrane concept from the two-dimensional continuum fluid to the partitioned fluid: High-speed single-molecule tracking of membrane molecules. *Annu. Rev. Biophys. Biomol. Struct. 34*, 351−378.
(67) Yamazaki, V., Sirenko, O., Schafer, R. J., and Groves, J. T. (2005) Lipid mobility and molecular binding in fluid lipid membranes. *J. Am. Chem. Soc. 127*, 2826−2827.
(68) Owen, D. M., Williamson, D., Rentero, C., and Gaus, K. (2009) Quantitative microscopy: Protein dynamics and membrane organization. *Traffic 10*, 962−971.
(69) Deverall, M. A., Gindl, E., Sinner, E.-K., Besir, H., Ruehe, J., Saxton, M. J., and Naumann, C. A. (2005) Membrane lateral mobility obstructed by polymer-tethered lipids studied at the single molecule level. *Biophys. J. 88*, 1875−1886.
(70) Glabe, C. G., and Kayed, R. (2006) Common structure and toxic function of amyloid oligomers implies a common mechanism of pathogenesis. *Neurology 66*, S74−78.
(71) Butterfield, S. M., and Lashuel, H. A. (2010) Amyloidogenic protein−membrane interactions: Mechanistic insight from model systems. *Angew. Chem., Int. Ed. 49*, 5628−5654.
(72) Knight, J. D., Williamson, J. A., and Miranker, A. D. (2008) interaction of membrane-buond islet amyloid polypeptide with soluble and crystalline insulin. *Protein Sci. 17*, 1850−1856.
(73) Gilead, S., Wolfenson, H., and Gazit, E. (2006) Molecular mapping of the recognition interface between the islet amyloid polypeptide and insulin. *Angew. Chem., Int. Ed. 45*, 6476−6480.